Abscisic Acid Drives Stomatal Closure through Increases in Hydrogen Peroxide in Distinct Subcellular Compartments Including Mitochondria

Running Head: ABA increases H_2O_2 in guard cell mitochondria

Anthony E. Postiglione and Gloria K. Muday*

Department of Biology and the Center for Molecular Signaling, Wake Forest University, Winston Salem, NC, USA 27109

*** Correspondence:**
Gloria Muday
muday@wfu.edu

One sentence summary: Genetically encoded biosensors and chemical probes revealed ABA-dependent increases in hydrogen peroxide, a reactive oxygen species with signaling activity, in guard cell cytoplasm and mitochondria.

Keywords: guard cell, reactive oxygen species, abscisic acid, mitochondria, respiratory burst oxidase homolog (RBOH)

The author(s) responsible for distribution of materials integral to the findings presented in this article in accordance with the policy described in the Instructions for Authors (https://academic.oup.com/plcell/pages/General-Instructions) is Gloria K. Muday (muday@wfu.edu)

Abstract

Abscisic acid (ABA) closes stomata to minimize transpiration and gas exchange in response to drought. ABA signaling increases accumulation of reactive oxygen species (ROS) in guard cells to drive stomatal closure. We used chemical dyes and genetically-encoded biosensors to identify the subcellular localizations where ABA increases hydrogen peroxide (H_2O_2) in guard cells. The general redox sensor, dichlorofluorescein (DCF), revealed ABA-driven ROS increases in distinct subcellular locations including chloroplasts, cytosol, and nuclei. ABA also increased fluorescence of both DCF and an H_2O_2-selective probe, Peroxy Orange 1, in mitochondria, which colocalize with Mitotracker Red. Whole cell and mitochondrial localized ABA-increased ROS signals were lost in an ABA-insensitive quintuple ABA receptor mutant and accentuated in an ABA-hypersensitive mutant. The ABA-induced ROS accumulation in mitochondria was lost in guard cells of mutants with defects in genes encoding H_2O_2 elevating respiratory burst oxidase homolog (RBOH) enzymes and reduced by treatment with the RBOH inhibitor VAS2870. ABA treatment of guard cells transformed with the genetically-encoded H_2O_2 reporter targeted to the cytoplasm, roGFP2-Orp1, and the mitochondrial targeted, mt-roGFP2-Orp1, revealed significant ABA-induced H_2O_2 increases. Furthermore, H_2O_2 treatment is sufficient to close stomata. These results reveal that ABA elevates H_2O_2 accumulation in guard cell cytosol and mitochondria to drive stomatal closure.

Introduction

Drought stress negatively impacts plant growth due to excess water loss, which is a growing concern for crop yields as a result of global climate changes that include increased drought (Fahad et al., 2017). Stomatal closure reduces excess water loss but also limits CO_2 entry, thereby negatively impacting the photosynthetic rate (Lamaoui et al., 2018). Due to this tradeoff, stomatal aperture must be tightly controlled (Nilson and Assmann, 2007). Reduction in guard cell turgor to close stomata is mediated by the drought hormone abscisic acid (ABA), which signals in guard cells during states of decreased water availability (Xu et al., 2016; Li et al., 2017; Qi et al., 2018; Qu et al., 2018; Tõldsepp et al., 2018).

The binding of ABA to the PYR/PYL/RCAR family of soluble receptors initiates ABA signaling (Park et al., 2009). The ABA bound receptors form a complex with Clade A protein phosphatases type 2C (PP2Cs), which negatively regulate ABA signaling in the absence of the hormone (Hsu et al., 2021). Formation of this complex inhibits PP2C activity, releasing the negative regulation of the pathway (Ma et al., 2009; Park et al., 2009; Nishimura et al., 2010). Reduced phosphatase activity allows for increased phosphorylation of a variety of proteins including Sucrose nonfermenting Related Kinase 2 family members (SnRK2s) (Takahashi et al., 2020). Active SnRK2s can then initiate a signaling cascade through phosphorylation of a number of downstream targets including Respiratory Burst Oxidase Homologs (RBOH) enzymes, also called NADPH oxidase (NOX) enzymes (Sirichandra et al., 2009). Consistent with RBOH activation, ROS accumulation in guard cells following ABA treatment has been observed in multiple plant species (Pei et al., 2000; Kwak et al., 2003; Watkins et al., 2014; Watkins et al., 2017). These elevated ROS act as second messengers to activate guard cell ion channels ultimately resulting in increased K^+ efflux and the reduction of guard cell turgor, which leads to stomatal closure (Geiger et al., 2009; Demidchik, 2018).

ROS bursts resulting from RBOH activation have been characterized in plants in response to a myriad of developmental and environmental signals (Chapman et al., 2019). These enzymes function in the production of extracellular superoxide through the transfer of electrons from NADPH or $FADH_2$ to molecular oxygen (Suzuki et al., 2011). Superoxide may be rapidly converted to H_2O_2 spontaneously or by enzymatic means via superoxide dismutases (Fukai and Ushio-Fukai, 2011). Extracellular H_2O_2 may then enter plant cells through plasma membrane

localized aquaporins (Bienert et al., 2007; Tian et al., 2016; Rodrigues et al., 2017). The Arabidopsis genome encodes 10 RBOH family members (RBOHA-RBOHJ) with distinct expression patterns and functions that regulate a variety of developmental and cellular processes (Chapman et al., 2019). Genetic approaches have identified a role of RBOHF during ABA-induced stomatal closure (Kwak et al., 2003). Both the *rbohf* single mutant and the *rbohd/f* double mutant had reduced ABA-driven increase in redox state and stomatal closure as compared to wild-type guard cells (Kwak et al., 2003).

ROS, most notably hydrogen peroxide (H_2O_2) and superoxide, play critical roles in signaling cascades in numerous organisms including plants (Foyer and Noctor, 2020). Prior studies examining ABA-dependent increases in ROS accumulation have largely examined changes in fluorescence of dichlorofluorescein (DCF) (Pei et al., 2000; Zhang et al., 2001; Kwak et al., 2003; An et al., 2016; Wu et al., 2017). However, since DCF is a general redox sensor, information on which types of ROS are increased by ABA cannot be inferred from this sensor (Kalyanaraman et al., 2012; Winterbourn, 2014). Additionally, the types of imaging used in previous studies prevented identification of the subcellular locations where these ROS increase during ABA signaling. Enzymes in plant cells that produce ROS in multiple subcellular locations have been identified (Noctor and Foyer, 2016).

Insight into the subcellular localization of where ROS accumulates in guard cells after ABA treatment, as well as the type of ROS that are increased are needed to understand how these molecules function in ABA signaling (Gadjev et al., 2006). Recent technological advances in both microscopic resolution and detection of ROS using chemical or genetically encoded sensors (Dickinson et al., 2010; Winterbourn, 2014; Nietzel et al., 2019; Ugalde et al., 2021a) have provided the ability to gain better insight into this spatial accumulation of different ROS species in response to environmental stresses, hormone signaling and development.

This study examined how ABA affects the accumulation and localization of H_2O_2 within Arabidopsis guard cells during the ABA response and how each of these intracellular compartments contribute to total ROS changes during stomatal closure. The subcellular distribution of the general redox sensor, DCF, was examined across multiple subcellular locations including the guard cell chloroplasts, cytosol, nuclei, and puncta within the cytosol. We used a dye that accumulates in mitochondria and a genetically-encoded H_2O_2 biosensor targeted

to the mitochondrial matrix to reveal that the puncta whose ROS accumulation increases after ABA treatment are mitochondria. To verify that the changes in ROS were directly tied to ABA signaling, we examined how mutations that block ABA signaling or accentuate signaling prevent or accentuate the ABA changes in DCF fluorescence. Both Peroxy Orange 1, a chemical probe selective for H_2O_2, and the roGFP2-Orp1 genetically encoded sensor were used to ask whether H_2O_2 increased and in what locations. This combination of chemical and genetic approaches reveals that ABA increases H_2O_2 accumulation in several guard cell locations including the cytosol and mitochondria and that ROS increases in guard cells are both necessary and sufficient for stomatal closure.

Results

ABA Significantly Increases DCF Fluorescence in Arabidopsis Guard Cells

To verify ABA-induced redox changes within Arabidopsis guard cells, we monitored fluorescence intensity changes using multiple ROS-responsive fluorescent probes. We began with CM 2,7-dihydrodichlorofluorescein diacetate (CM H_2DCF-DA), which is a frequently utilized fluorescent chemical probe to monitor changes in redox state (Halliwell and Whiteman, 2004). CM H_2DCF-DA diffuses across the plasma membrane, where it is trapped within the cell after cleavage by cellular esterases (Swanson et al., 2011). The probe is then converted to highly fluorescent DCF upon oxidation by ROS. Whole leaves of Col-0 were excised in the early morning, epidermal peels were prepared, and then covered with a stomatal opening solution for 3 hrs under white light to fully open stomata. This was followed by incubation with 20 µM ABA or a control treatment for 45 min. Treatments were then removed and leaf peels were incubated with CM H_2DCF-DA for 15 min. Figure 1 shows laser scanning confocal microscope (LSCM) images of guard cells with control or ABA treatment with the images of DCF fluorescence are shown directly and after conversion to lookup tables (LUT), which clarifies the range of fluorescence across these cells. Whole stomata DCF fluorescence was recorded in 30 or more stomata per treatment and each individual value was normalized relative to the average signal intensity of control treated stomata (Figure 1B). This quantification revealed that ABA significantly increased DCF fluorescence in guard cells during ABA-induced stomatal closure.

ABA Signaling Mutants Display Differences in Guard Cell ROS Accumulation

To determine whether the increased DCF accumulation seen following ABA treatment occurred via the canonical ABA signaling pathway, we examined two Arabidopsis mutant lines that have altered ABA sensitivity. An ABA receptor quintuple mutant *pyl1-1*; *pyr1-1*; *pyl4-1*; *pyl5*; *pyl8-1* (abbreviated *pyl-11458*) which has impaired ABA sensitivity (Zhang et al., 2020) and ABA overly sensitive 6 (*abo6),* which displays increased ABA response in primary root inhibition linked to a mutation in a mitochondrial DEXH box RNA helicase (He et al., 2012). To examine ABA sensitivity in both of these genotypes, we compared stomatal closure in Col-0, *pyl-11458*, and *abo6* guard cells following treatment with ABA. Leaves were excised and peeled and then covered with stomatal opening buffer for 3 hrs as described previously. Epidermal peels were

Figure 1

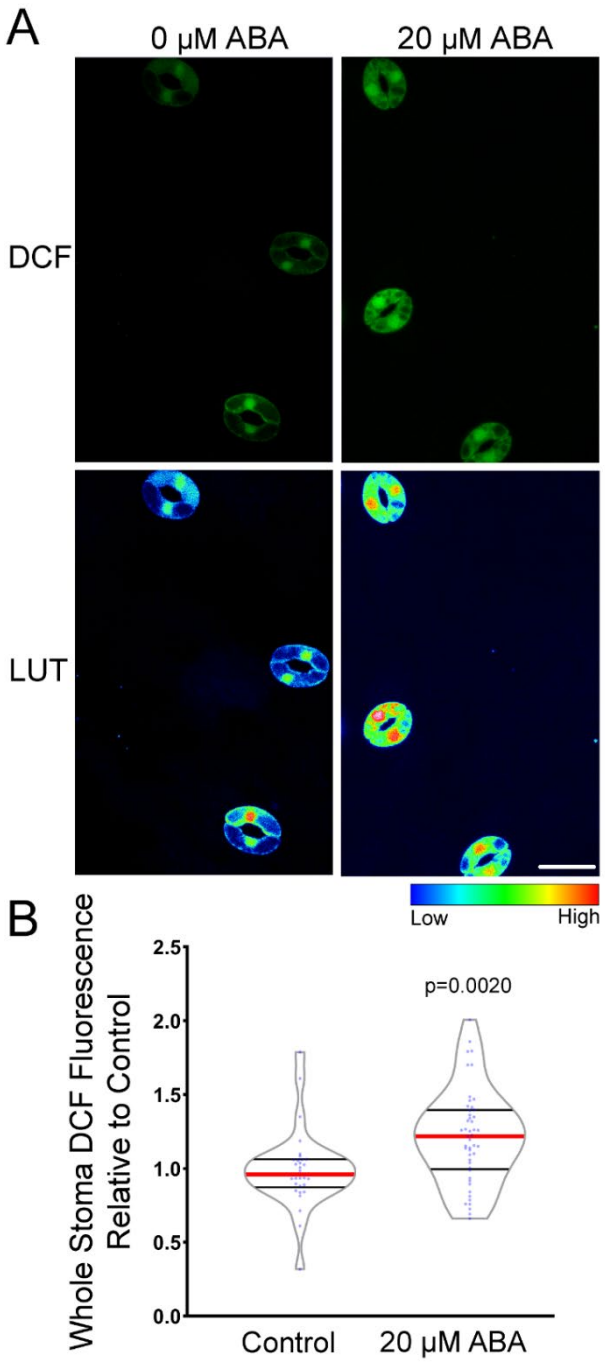

Figure 1. ABA increases DCF fluorescence within Arabidopsis guard cells.
A) Confocal micrographs of DCF fluorescence of Arabidopsis guard cells treated with buffer control or 20 µM ABA for 45 min shown directly or after conversion to lookup tables (LUT). Scale bar: 20µm. B) Violin plot showing quantifications of DCF fluorescence in the entire guard cell with and without ABA treatment in 30-50 whole stomata per treatment from three separate experiments. All individual values were normalized to the average of the control treatment and are displayed on the graph as blue dots with the median shown in red and lower and upper quartiles indicated in black. P-values from paired student t-tests for samples compared to untreated controls are reported.

then treated with 20 μM ABA or control buffer for 45 min and guard cells were immediately imaged (Figure 2). Representative images are shown in Figure 2A and stomatal apertures of at least 90 stomata per genotype for each time point were quantified over three separate experiments (Figure 2B). Initial apertures after incubation in opening solution were not significantly different between Col-0, *pyl-11458,* and *abo6.* Consistent with altered ABA response in these mutants, *pyl-11458* showed a significant reduction in ABA-dependent closure, while *abo6* showed a significant increase in ABA dependent closure relative to Col-0.

We also examined ABA-dependent DCF fluorescence increases in these mutants under the same conditions described above and provide images of DCF fluorescence converted to LUT (Figure 2C). Under control conditions, guard cells of *pyl-11458* and *abo6* had similar levels of DCF fluorescence to Col-0 (Figure 2C-D). However, the significant increase in whole guard cell DCF fluorescence following ABA-treatment in Col-0 was absent in the *pyl-11458* mutant whose DCF signal was not significantly changed by ABA, consistent with its impaired stomatal closure. In contrast, treatment of *abo6* with ABA increased DCF fluorescence in this mutant to levels that were 1.2-fold higher than Col-0 guard cells under the same treatment conditions, suggesting that enhanced ROS accumulation in this mutant drives the enhanced stomatal closure response. These findings are consistent with ABA signaling driving ROS increases in guard cells and with the degree of ABA sensitivity being directly correlated with the amount of ROS production in these genotypes.

ABA Drives Compartmentalized ROS Increases within Guard Cells

The images in Figure 1A and 2C suggest that ABA increases DCF signal in a range of distinct subcellular localization. We therefore performed higher resolution imaging of individual guard cells to identify where within the cell ABA increases ROS. Figure 3 reveals that ABA treatment increased DCF fluorescence within multiple subcellular regions. The DCF signal increases in the chloroplast and nucleus were verified through spectral unmixing of the DCF signal from chlorophyll autofluorescence and DAPI fluorescence, respectively (Supplemental Figure S1A-B). DCF fluorescence is largely excluded from the vacuole, but there are increases in DCF signal after ABA treatment in the cytosol and small cytosolic punctate structures (Figure 3A), which we identified as mitochondria in experiments described in Figure 4. To determine how each of these

Figure 2

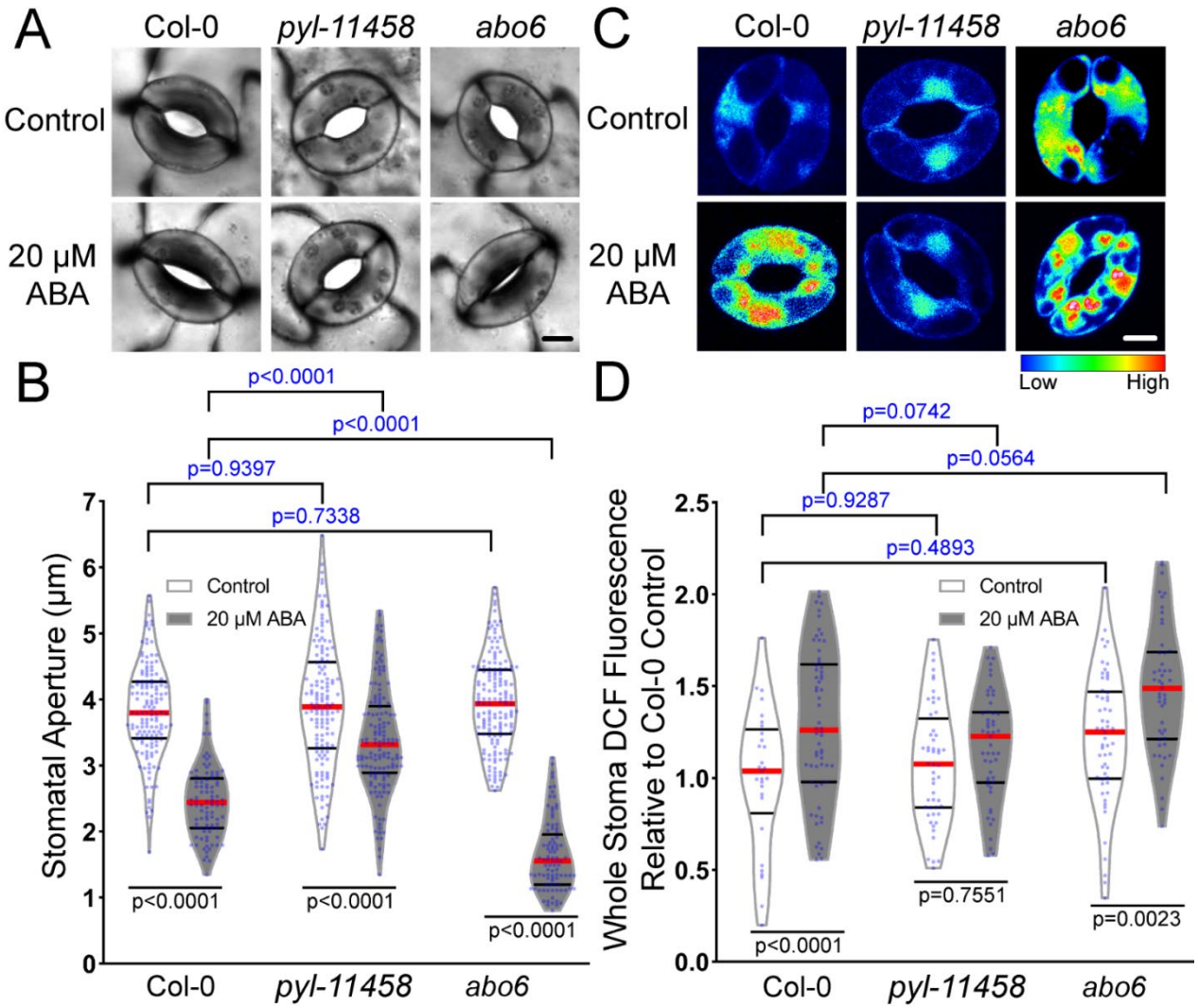

Figure 2. ABA signaling mutants have altered ABA-dependent guard cell closure and differences in DCF fluorescence. A) Stomatal apertures of leaves of Col-0, the *pyl-114588* quintuple mutant (*pyr1;pyl1;pyl4;pyl5;pyl8)*, and *abo6* are shown following treatment with control or 20 µM ABA for 45-min. B) Stomatal apertures of Col-0, *pyl-114588*, and *abo6* leaves were quantified with and without ABA treatment for 45 min. C) Confocal micrographs of DCF fluorescence converted to lookup tables (LUT) of Col-0, *pyl-114588,* and *abo6* cells treated with buffer or 20 µM ABA. D) Violin plot showing quantification of DCF fluorescence in the entire guard cell of each genotype with and without ABA treatment from three separate experiments All individual values were normalized to the average of the control treatment in Col-0 and are displayed on the graph as blue dots with the median shown in red and lower and upper quartiles indicated in black. B and D) The p-values in blue font above the violin plot reveal differences between genotypes within treatments, while the p-values in black font shown below the plot represent the statical significance of differences between treatments in the same genotype. The reported p-values are from a one-way ANOVA followed by Tukey's post hoc test from three separate experiments examining 50-62 stomata/sample. Scale bar: 5µm.

Figure 3

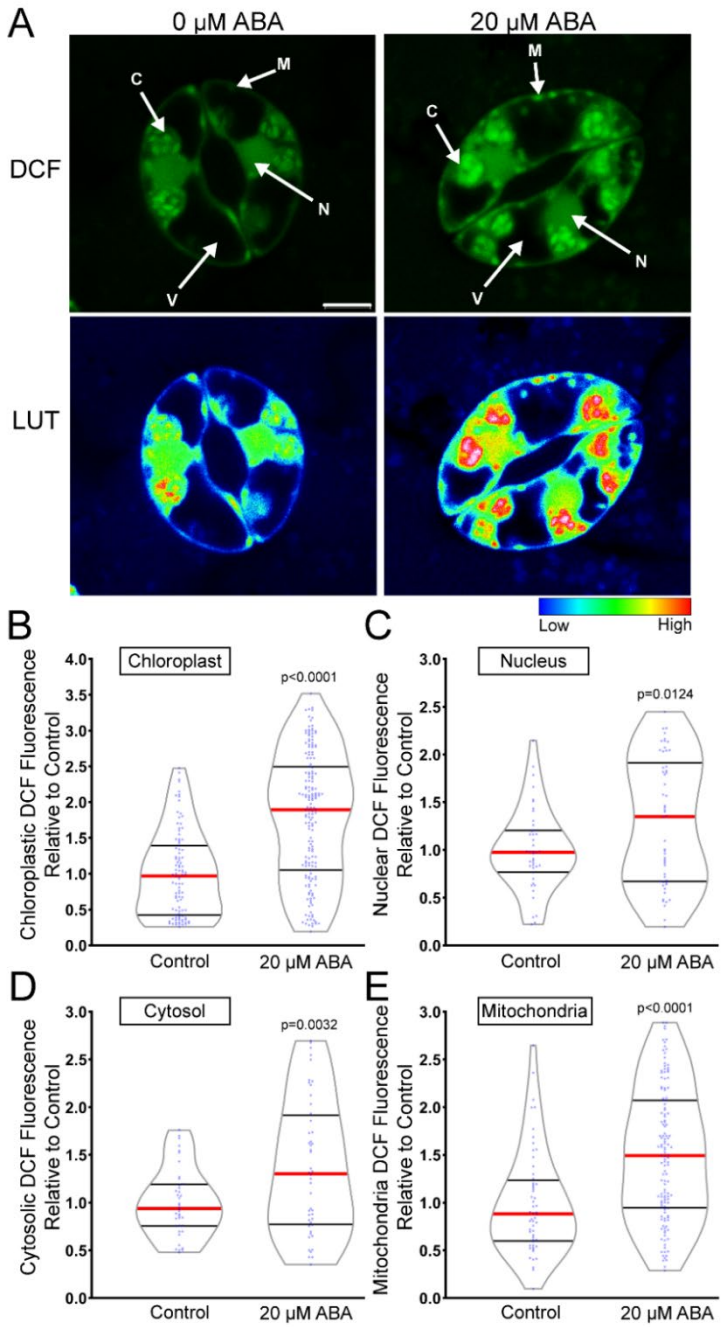

Figure 3. ABA increases DCF fluorescence in several locations within Arabidopsis guard cells.
A) Confocal micrographs of DCF fluorescence shown directly or after conversion to LUT for Arabidopsis guard cells treated with buffer or 20 µM ABA. Subcellular compartments are indicated on each image (C: Chloroplast, N: Nucleus, M: Mitochondria, V: Vacuole). Scale bar: 5µm. Quantifications of DCF fluorescence in the B) chloroplast, C) nucleus, D) cytosol and E) mitochondria with and without ABA treatment from three separate experiments with each bar represented by (chloroplast n>100, nuclear n>48, cytosol n>48 and mitochondria n>56). All individual values were normalized to the average of the control treatment for each subcellular location and are displayed on the graph as blue dots with the median shown in red and lower and upper quartiles indicated in black. The p-values were generated by student t-tests comparing ABA to control in each cellular location.

subcellular regions contribute to overall ROS changes, we quantified increases in each of these locations. Following 45 minutes of 20 µM ABA treatment, we observed the largest increase within the chloroplasts at 1.8-fold over untreated guard cells (Figure 3B). We also observed significant increases in other locations with a 1.3-fold ABA-induced increase within guard cell nuclei (Figure 3C), a 1.4-fold increase in the cytosolic signal (Figure 3D), and a 1.5-fold increase in mitochondrial signal (Figure 3E).

To determine whether the differences in DCF fluorescence between subcellular locations was a function of differential dye uptake rather than changes in redox state, we monitored uptake of a non-oxidizable variant of DCF, fluorescein diacetate (FDA). This probe displayed the same localization as DCF (Supplemental Figure S1C), which is consistent with increases in DCF fluorescence that proceed ABA treatment being due to changes in redox state and not differential dye uptake. These data suggest that ABA increased ROS in many intracellular locations within guard cells. As RBOH enzymes have been implicated in ABA-induced ROS accumulation, we next asked whether ABA-induced ROS increases in all of these subcellular locations are dependent on RBOH enzymes.

ABA Increases H_2O_2 in Subcellular Regions Including Chloroplasts and Mitochondria to Induce Stomatal Closure

We utilized the H_2O_2-selective chemical probe Peroxy Orange 1 (PO1) (Dickinson et al., 2010) to ask whether ABA increased H_2O_2. PO1 is a membrane-permeable, boronate-based probe that is non-fluorescent in its reduced form, which becomes fluorescent upon irreversible oxidation by H_2O_2. The spectral profile of PO1 was isolated and unmixed from leaf auto-fluorescence including chloroplasts and the signal in the absence and presence of 20 and 100 µM ABA is shown in Supplemental Figure S2A. Treatment with 20 µM ABA significantly increased PO1 signal in the chloroplasts but did not result in a significant increase in the nucleus, cytosol, or mitochondria (Supplemental Figure S2B-E). To determine if higher concentrations of ABA were sufficient to stimulate H_2O_2 increases throughout guard cells, we increased concentration of ABA to 100 µM.

We quantified PO1 in the cytosol, nucleus, chloroplasts, and mitochondria of guard cells. Following treatment with 100 µM ABA, we observed significant increases in PO1 signal in

chloroplasts (Supplemental Figure S2B). Treatment with 100 µM ABA also resulted in a small, but significant increase in PO1 signal within mitochondria (Supplemental Figure S2E). After treatment with 100 µM ABA treatment, PO1 signal within the cytosol and nucleus were not significantly different from control treatments (Supplemental Figure S2C-D). This suggests that PO1 may not be taken up by all organelles or that PO1 may not be sensitive enough to detect small changes in guard cell H_2O_2.

To verify that PO1 fluorescence is ROS responsive in the nucleus, we treated guard cells with 250 µM exogenous H_2O_2 (Supplemental Figure S3A-C). Treatment with exogenous H_2O_2 resulted in a 1.5-fold increase in nuclear PO1 fluorescence indicating that PO1 can be sufficiently taken up by Arabidopsis guard cell nuclei to detect large increases in H_2O_2 (Supplemental Figure S3C). This raises the possibility that ABA-induced increases in H_2O_2 in guard cells may need more sensitive tools for their detection. Additionally, the effect of this exogenous H_2O_2 treatment on guard cell closure was quantified in Supplemental Figure S3B. Treatment with exogenous H_2O_2 for 30 minutes was sufficient to close stomata to levels consistent with ABA-dependent closure.

In the chloroplast, we observed ABA-induced PO1 accumulation into distinct structures within inner chloroplast compartments. However, two-dimensional images of maximum intensity projection make it difficult to discern if these dyes are associated with the chloroplast membrane, or internal to this organelle. Therefore, we created three-dimensional renderings of PO1 labeled guard cells to gain insight into chloroplast PO1 distribution (Supplemental Figure S4). These renderings show that bright PO1 regions span the chloroplast and are not just on the surface, revealing a complex ROS accumulation pattern within the chloroplast while the mitochondria are circular structures with uniform PO1 signal. It is worth noting that the PO1 localized signal is similar in position and size to the accumulation of starch grains (Leshem and Levine, 2013) (Supplemental Figure S4).

ABA Treatment Results in DCF Increases within Guard Cell Mitochondria

DCF and PO1 localized to small cytosolic punctate structures in addition to chloroplasts and nuclei. We used colocalization of chemical ROS probes with fluorescent organelle dyes and an organelle targeted GFP to ask whether these puncta are ROS producing peroxisomes or

mitochondria (Figure 4). To evaluate whether cytosolic ROS puncta were peroxisomes, we examined an Arabidopsis transgenic line with a GFP tagged with a type 1 peroxisomal targeting signal (GFP-PTS1) (Ramón and Bartel, 2010) (Figure 4A). GFP-PTS1 and PO1 have emission peaks that can be spectrally unmixed. We used the Zen colocalization module to draw ROIs around cytosolic punctate structures that did not overlay on a chloroplast (Figure 4B). Although the GFP-PTS1 signal accumulated into punctate structures within the guard cell cytosol, they did not colocalize with the puncta labeled with PO1 (Figure 4C).

To determine whether these puncta colocalize with mitochondria, we labeled Col-0 guard cells with Mitotracker Red prior to staining with CM H_2DCF-DA. Figure 4D shows Mitotracker (magenta), DCF signal (green), and chlorophyll signal (red), separately and in an overlay. All of the DCF puncta appeared to contain Mitotracker red signal. We drew ROIs around more than 40 DCF puncta (Figure 4E). Also, these structures display higher PO1 intensity than most other localizations which allowed us to use the lowest intensity puncta to define the colocalization threshold and generate a colocalization graph (Figure 4F). A majority of pixels in the designated ROIs contain both DCF and Mitotracker Red signals and we calculated the average weighted colocalization coefficient to be 0.96. These results demonstrate the ABA-increased ROS puncta in guard cells are mitochondria.

Mutants with Altered ABA Signaling Show Changes in Mitochondrial ROS

Since the nature of the *abo6* mutation results in increased mitochondrial ROS accumulation in Arabidopsis roots (He et al., 2012), we examined the effect of ABA on mitochondrial ROS in *abo6* (Supplemental Figure 5). We found that *abo6* contained significantly higher levels of ROS in guard cell mitochondria following both ABA and control treatments when compared to Col-0. Altogether, these results are consistent with ABA-driven increases in H_2O_2 within guard cell mitochondria via canonical ABA signaling pathways that contribute to ABA-dependent stomatal closure.

Figure 4

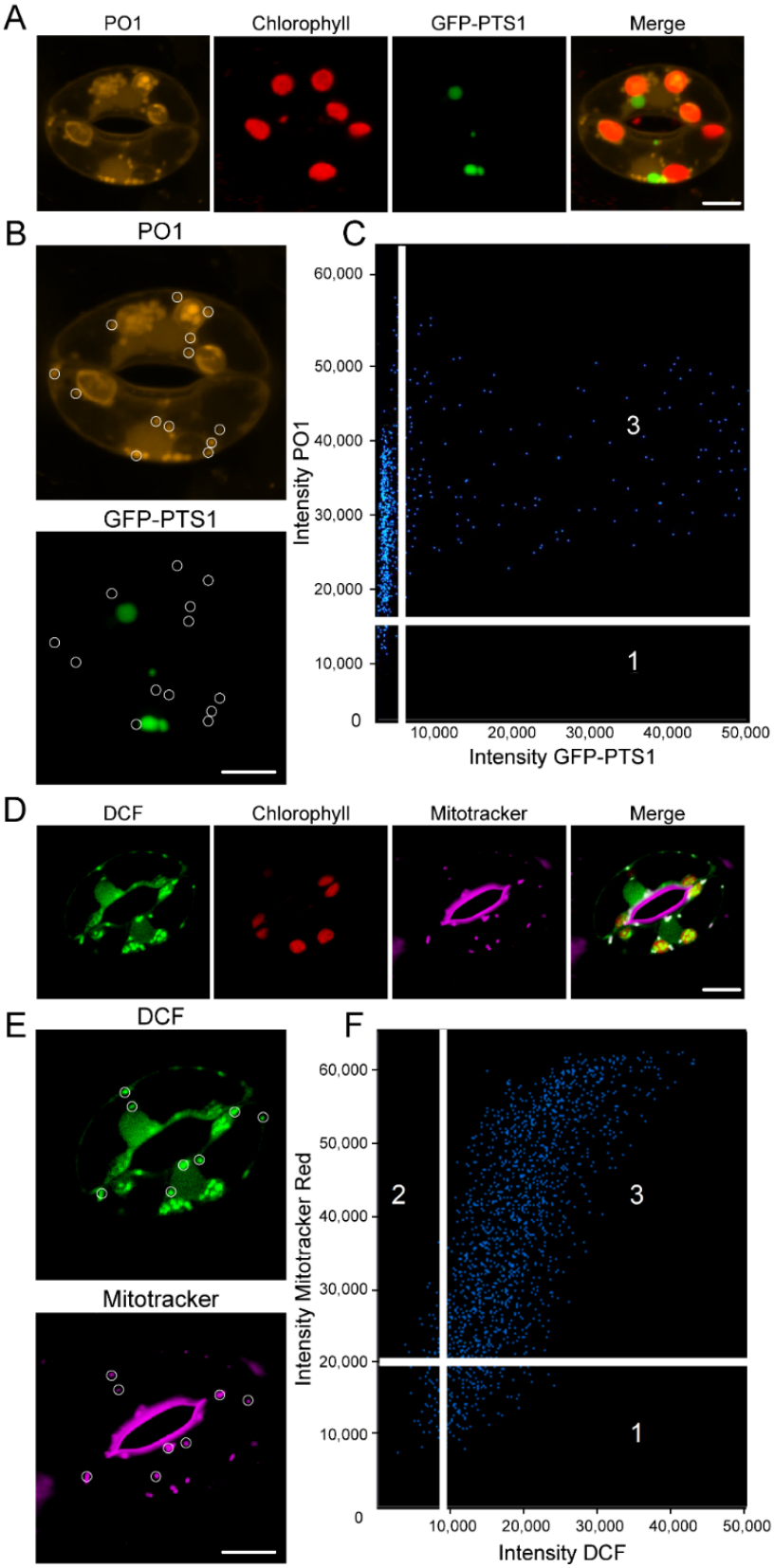

Figure 4. ABA treatment results in increased ROS accumulation in cytosolic puncta that colocalize with mitochondria. A) Confocal micrographs of PO1 fluorescence (orange), chlorophyll autofluorescence (red), PO1 fluorescence and GFP-PTS1 (green), and a merged image. Maximum intensity projection of full z-stack is shown. B) Regions of interest used to generate weighted colocalization coefficient are circled in white, highlighting the absence of PO1 fluorescence colocalizing with GFP-PTS1 fluorescence. C) Colocalization graph generated with the ZEN Black colocalization module from regions of interest highlighting PO1-labeled cytosolic puncta. D) Confocal micrographs of DCF fluorescence (green), chlorophyll autofluorescence (red), Mitotracker Red (magenta), and a merged image showing DCF colocalized with Mitotracker Red (white). Individual optical slices of the same guard cells are shown. E) Regions of interest used to generate weighted colocalization coefficient are circled in white, showing DCF fluorescence colocalizing with Mitotracker Red fluorescence. F) Colocalization graph generated with the ZEN Black colocalization module from regions of interest highlighting DCF-labeled cytosolic puncta. Scale bars: 5µm.

Mutants Deficient in *rbohd* and *rbohf* Have Impaired ABA-Induced ROS Accumulation in Several Subcellular Locations

RBOH enzymes are well-characterized producers of signaling ROS that regulates a myriad of plant developmental processes and environmental responses (Chapman et al., 2019). To determine whether RBOH enzymes are required for the increase in ROS accumulation in the cytosol and other cellular localizations following ABA treatment, we examined DCF fluorescence in Arabidopsis mutants with defects in the genes encoding RBOHD and RBOHF (Figure 5), which were previously reported to function in ABA-induced stomatal closure (Kwak et al., 2003). Figure 5A contains images of DCF fluorescence reported as lookup tables in Col-0 and the double mutant *rbohd/f*. The striking ABA-induced increase in nuclear DCF signal in Col-0 is clearly diminished in this mutant. To ask whether this effect is significant, as well as changes in chloroplast, cytosol, and mitochondria, we quantified DCF fluorescence in each of these locations. The *rbohd/f* double mutant not only exhibited reduced DCF accumulation in the cytosol following 20 µM ABA treatment for 45 minutes (as predicted by the known function of RBOH proteins in controlling cytosolic ROS), but we also observed a significant reduction in signal in chloroplasts, nuclei, and mitochondria (Figure 5B-E). We also utilized the pan NADPH-oxidase (NOX) inhibitor VAS2870. This compound selectively targets an active-site cysteine that is conserved in mammalian NOX enzymes as well as plant RBOHs (Yun et al., 2011). We confirmed that VAS2870 regulated ABA responses in guard cells by evaluating its effect on ABA-induced stomatal closure. Pre-treatment with 10 µM VAS2870 for 1 hr prior to ABA treatment was able to significantly inhibit ABA-dependent stomatal closure compared to guard cells treated with ABA alone, suggesting it is an effective RBOH inhibitor in guard cells (Supplemental Figure S6A-B) and supporting the requirement of RBOH activity for full ABA-induced stomatal closure.

Pre-incubation with VAS2870 resulted in a significant dampening in the ABA-dependent DCF increase in the chloroplasts, although ABA still had a small, but significant effect on DCF signal in this organelle when compared to control guard cells ($p=0.0155$) (Figure 5B). VAS2870 abolished ABA-induced ROS increases in both the cytosol and mitochondria, while the ABA-increased DCF signal in the nucleus was not significantly different from control treated cells or

Figure 5

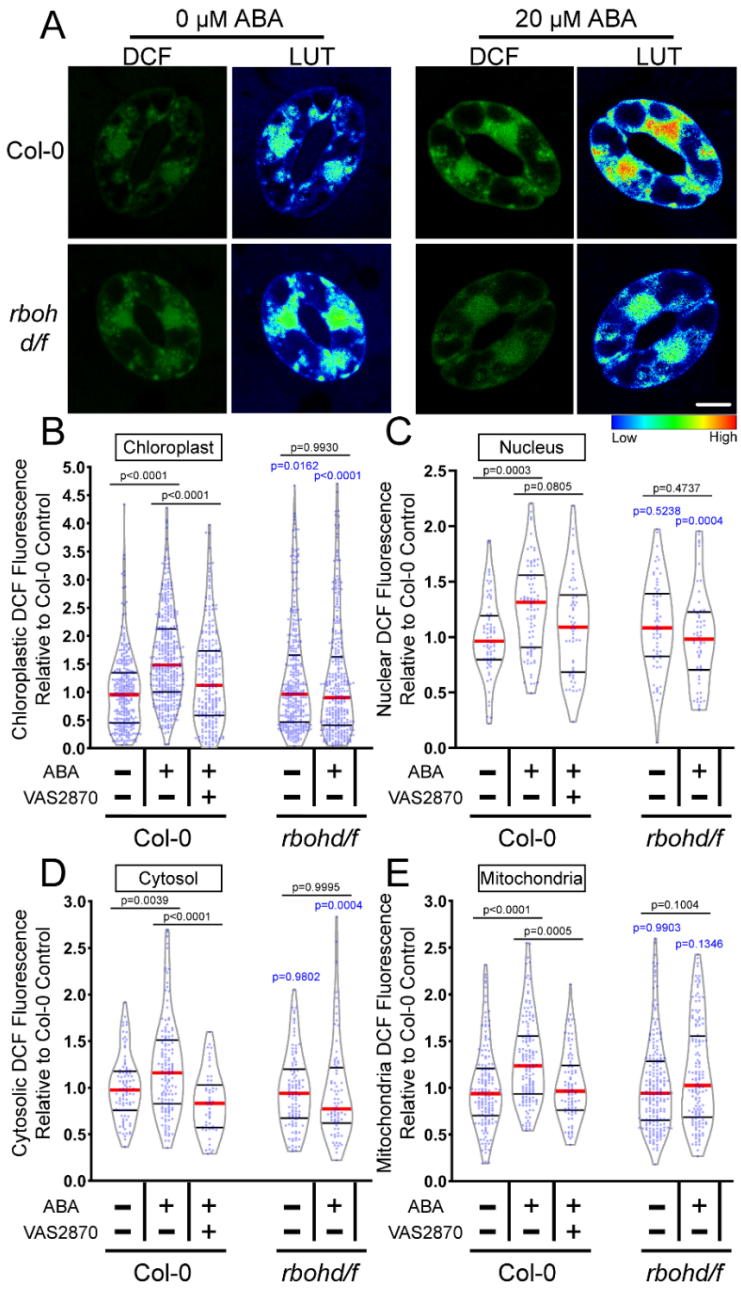

Figure 5. RBOH enzymes contribute to ABA-increased ROS accumulation in several subcellular localizations. A) Confocal micrographs of DCF fluorescence or DCF images converted to LUT of Col-0 or *rbohd/f* guard cells treated with buffer control or 20 µM ABA. Scale bar: 5µm. Violin plots show quantifications of DCF fluorescence in the B) chloroplast, C) nucleus, D) cytosol and E) mitochondria following treatment with control buffer, ABA, or pre-treated with VAS2870 and then treated with ABA from three separate experiments (chloroplast n>239, nuclear n>59, cytosol n>52 and mitochondria n>85). All individual values were normalized to the average of the control treatment in Col-0 for each subcellular location and are displayed on the graph as blue dots with the median shown in red and lower and upper quartiles indicated in black. P-values in black font represent the significance of differences between treatments in the same genotype spanning the compared treatments. P-values in blue font representing the significance of differences between the indicated genotypes and Col-0. P-values are recorded according to one-way ANOVA followed by Tukey's post hoc test.

those treated with ABA alone (Figure 5C-E and Supplemental Figure S6). Altogether, these findings are consistent with RBOH enzymes driving ABA-dependent ROS accumulation in multiple subcellular compartments in Arabidopsis guard cells, which are required for guard cell closure. Since DCF is oxidized by multiple ROS, our next step was to use a dye with greater specificity toward H_2O_2, which plays an important role in cell signaling.

The Genetically-Encoded ROS Biosensor roGFP2-Orp1 Showed Rapid ABA-Dependent H_2O_2 Increases Within Guard Cell Nuclei and Cytosol

The inability to identify increases in H_2O_2 in the cytoplasm using PO1 suggested that a more sensitive detection approach was needed. Therefore, we further evaluated changes in H_2O_2 using the genetically encoded biosensor, roGFP2 linked to yeast Orp1, which has enhanced sensitivity relative to chemical probes (Nietzel et al., 2019). In the presence of H_2O_2, the yeast peroxidase Orp1 protein (also known as glutathione peroxidase 3) becomes oxidized to sulfenic acid (Cys-SOH) on a reactive cysteine residue that rapidly forms an intramolecular disulfide bond with a nearby cysteine. This disulfide is then efficiently transferred via thiol-disulfide exchange to a pair of cysteines on roGFP2, resulting in a conformational change that alters the optical properties of the fluorophore (Gutscher et al., 2009). When reduced, the sensor has increased signal intensity after excitation with the 488 nm laser line, while oxidation leads to elevated signal following 405 nm excitation. Therefore, dividing signal intensity after 405 nm excitation by intensity following 488 nm excitation provides a ratiometric readout which has an internal control for expression levels within a particular tissue.

To examine the effect of ABA on oxidation of this sensor, we excised fully mature Arabidopsis leaves containing roGFP2-Orp1 and generated epidermal leaf peels as described above (Figure 6). The process of generating an epidermal leaf peel is a mechanical stress, that increased roGFP2-Orp1 oxidation. We verified that incubation of the epidermal leaf peels in stomatal opening buffer for 4 hrs prior to any treatment allowed oxidation to begin returning to baseline levels, consistent with a prior report (Scuffi et al., 2018). Stomatal opening buffer was removed following equilibration and replaced with a similar solution containing 100 µM ABA or a control treatment for 45 min. Figure 6A shows the fluorescence of roGFP2-Orp1 guard cells excited at either 405 or 488 and illustrates that consistent with oxidation of this reporter after ABA treatment, the fluorescence of a sample excited at 405 is elevated and the fluorescence of the

sample excited at 488 is reduced. The increase in oxidation after ABA treatment is most evident when the ratio of fluorescence at these two excitations is reported (Figure 6A). We quantified the effect of ABA treatment in roGFP2-Orp1 oxidation in whole stomata, which resulted in a 1.3-fold increase in oxidation ratio when compared to control guard cells (Figure 6A-B).

To demonstrate the dynamic range of this sensor, we treated with 20 mM DTT to reduce this biosensor, which leads to a low 405/488 fluorescence ratio (Figure 6C), with direct fluorescence images also shown in Supplemental Figure S7. In contrast, treatment with H_2O_2 increases protein oxidation leading to an elevated 405/488 fluorescence ratio. The dynamic range of the sensor as judged by DTT and H_2O_2 treatment defining the minimum and maximum is noted on the graph in Figure 6C. These data are consistent with ABA driving an increase in guard cell H_2O_2 during stomatal closure.

A benefit of using this genetically encoded sensor is the ability to monitor changes in H_2O_2 within individual guard cells over time to gain insights into the spatial dynamics of ABA-dependent increases in H_2O_2. The changing sensor oxidation over time in a single guard cell treated with ABA followed by a treatment with DTT, to reverse this oxidation, is shown in Supplemental Figure S8A. The challenge of continuous illumination of the same guard cells is that it can lead to light-induced oxidation of the sensor due to excitation of chloroplasts leading to increases in H_2O_2 (Ugalde et al., 2021b). Consistent with this prior report, we can initially detect differences in sensor oxidation between ABA treated and buffer control samples, but after 30 minutes of imaging, the amount of oxidation of the sensor in the control became similar to the ABA-induced oxidation (Supplemental Figure S8B). Therefore, we imaged multiple samples at several time points as described for the chemical probes above.

To examine the temporal dynamics of H_2O_2 accumulation within the cytosol and nucleus following ABA treatment, we monitored oxidation shifts in guard cells transformed with roGFP2-Orp1 by drawing ROIs in these locations. Although this variant of roGFP2-Orp1 is targeted to the cytosol, the biosensor also shows signal in the guard cell nucleus (Nietzel et al., 2019; Babbar et al., 2021), allowing us to also monitor H_2O_2 changes in this organelle. Leaves expressing roGFP2-Orp1 were peeled and equilibrated in stomatal opening solution as described above. Opening buffer was then removed following equilibration and replaced with 100 µM

Figure 6

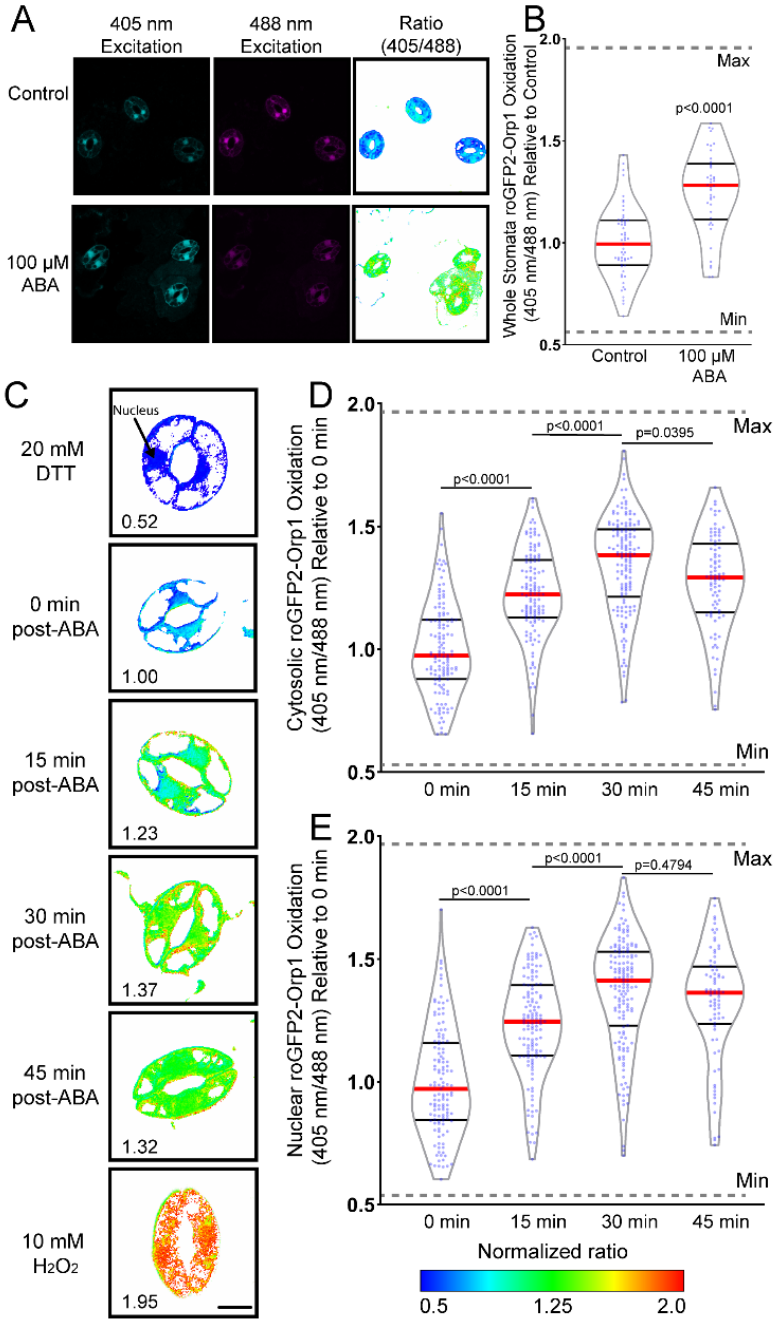

Figure 6. roGFP2-Orp1 is able to detect ABA-increased H_2O_2 within the guard cell cytosol and nuclei. A) Confocal micrographs of Arabidopsis guard cells expressing roGFP2-Orp1 treated with 100 µM ABA for 45 min. Ratiometric images display fluorescence ratios calculated from images taken using sequential excitation at 488 nm and 405 nm for each treatment group. B) Quantification of intracellular roGFP2-Orp1 ratios following 100 µM ABA or control treatment. Ratios are calculated by dividing fluorescence intensity collected at emission window 500-535 nm after excitation at 405 nm by the intensity collected in the same emission window after 488 nm excitation. All individual values were normalized to the average of the control treatment and are displayed on the graph as blue dots with the median shown in red and lower and upper quartiles indicated in black with data from three separate experiments (n=42-57 whole stomata for each treatment). P-values were calculated from student t-test. C) Confocal micrographs of Arabidopsis guard cells expressing roGFP2-Orp1 treated with 100 µM ABA for 0, 15, 30, 45 min. Minimum and maximum sensor oxidation are shown by treatment with 20 mM DTT or 10 mM H_2O_2, respectively. Ratios are calculated as above. Normalized ratios are then created relative to the average for the 0 min timepoint. D) Quantification of roGFP2-Orp1 ratio in the cytosol and E) nucleus following 100 µM ABA for 0, 15, 30, or 45 min. Data are reported from three separate experiments (n>80 guard cells for each time point). Minimum and maximum sensor oxidation is represented on graphs by gray dashed lines. The significance of differences between indicated time points were determined by one-way ANOVA followed by a Tukey's multiple comparisons test and are shown on the graph. Scale bar: 5µm.

ABA for 0, 15, 30, or 45 min (Figure 6C). Though roGFP2-Orp1 was still slightly oxidized in both the cytosol and nucleus after 4 hr incubation in stomatal opening solution, treatment with 100 µM ABA resulted in a significant increase in oxidation above baseline in both locations within 15 min (Figure 6D-E). ABA treatment led to continued oxidation of the sensor in a time-dependent manner, reaching a maximum of 1.3-fold increase over control in the cytosol and 1.4-fold in the nucleus at 30 min with signal starting to return to baseline at 45 mins (Figure 6C-E). These results use a sophisticated biosensor to demonstrate that ABA increases H_2O_2 with similar kinetics to ABA-dependent stomatal closure.

ABA Treatment Increases the Oxidation of Mitochondrial Targeted roGFP2-Orp1

To confirm that ABA perception drives H_2O_2 accumulation in guard cell mitochondria, we examined a transgenic line expressing roGFP2-Orp1 specifically in the mitochondrial matrix (mt-roGFP2-Orp1) (Nietzel et al., 2019) (Figure 7). To minimize oxidation due to generation of the leaf peel, we again equilibrated samples in stomatal opening solution for 4 hours before imaging. We again determined the dynamic range of this reporter using DTT to fully reduce the reporter and H_2O_2 to fully oxidize it, as shown in Figure 7A. It is evident that the signal of this reporter is dispersed in puncta throughout the cytosol, which is most evident in the H_2O_2 treated samples. This is consistent with the distribution of mitochondria revealed by Mitotracker Red.

Treatment with ABA resulted in a significant increase in this mitochondrial sensor 45 minutes after ABA treatment (Figure 7B) The magnitude of the ABA-dependent oxidation of mt-roGFP2-Orp1 is less pronounced than the cytosolic sensor, but it is evident that the signal shows a broader range across the cell and mt-roGFP2-Orp1 oxidation state across the entire mitochondrial population may not be as uniform as previously seen in the sensor targeted to the cytoplasm (Figure 7A). Additionally, we did not observe significant increases in oxidation at the 15- or 30-minute timepoints after ABA treatment (Supplemental Figure S9), which may reflect either reduced sensitivity of this sensor relative to the version targeted to the cytosol or that the changes in ROS in the cytosol precede change in the mitochondria. Since GFP signal is easily unmixed from that of PO1 emission, we used to this sensor to verify that PO1 labeled puncta were also identified as mitochondria through colocalization of these two signals (Supplemental Figure S10).

Figure 7

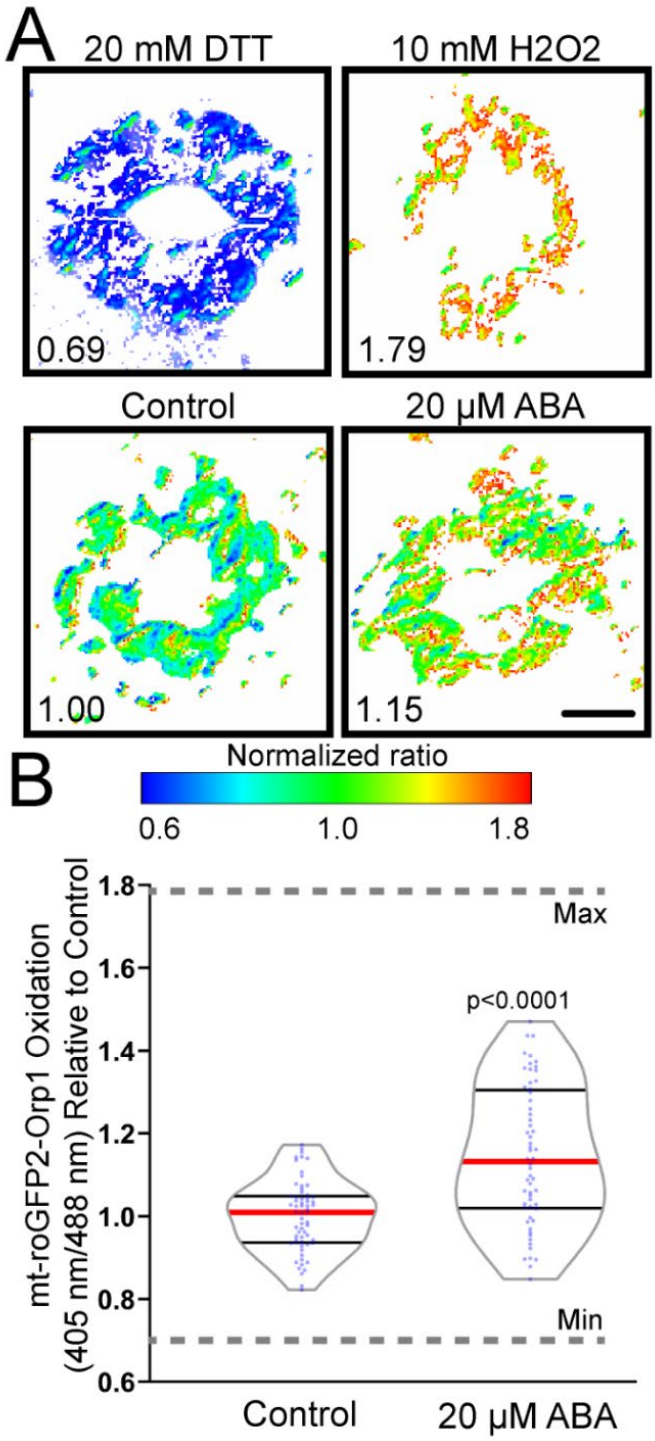

Figure 7. roGFP2-Orp1 targeted to guard cell mitochondria shows ABA-dependent H_2O_2 increases. A) Confocal micrographs of Arabidopsis guard cells expressing mt-roGFP2-Orp1 treated with 100 µM ABA or control buffer for 45 min. Ratiometric images display fluorescence ratios calculated from separate images taken using sequential excitation at 488 nm and 405 nm for each time point. Ratios are calculated by dividing fluorescence intensity collected at emission window 500-535 nm after excitation at 405 nm by the intensity collected in the same emission window after 488 nm excitation. Scale bar: 5µm. B) Quantification of mt-roGFP2-Orp1 ratio in the entire guard cell following 100 µM ABA or buffer control for 45 min. All individual values were normalized to the average of the control treatment and are displayed on the graph as blue dots with the median shown in red and lower and upper quartiles indicated in black. Minimum and maximum sensor oxidation are shown by treatment with 20 mM DTT or 10 mM H_2O_2, respectively. Data are reported from three separate experiments (n>60 stomata). Minimum and maximum sensor oxidation is represented on graphs by gray dashed lines. Listed p-values were determined by one-way ANOVA followed by Tukey's post hoc test. Scale bars: 5µm.

Discussion

Plants regulate stomatal aperture in response to environmental and hormonal signals through the control of guard cell turgor pressure (Nilson and Assmann, 2007). During drought stress, plants increase ABA synthesis (Boominathan et al., 2004), which initiates a complex signaling pathway that ultimately leads to stomatal closure (Vishwakarma et al., 2017). Included in this signaling cascade is the activation of RBOH enzymes that trigger a burst of ROS that act as second messengers in guard cell closure (Kwak et al., 2003). The accumulation of ROS following ABA treatment has been detected primarily by increases in DCF fluorescence, a nonspecific chemical ROS sensor, with signal quantified across the whole guard cell (Pei et al., 2000; Watkins et al., 2014; Watkins et al., 2017; Postiglione and Muday, 2020). However, technological advances in microscopic resolution as well as ROS detection, using both chemical and genetically encoded biosensors (Winterbourn, 2014; Nietzel et al., 2019; Ugalde et al., 2021a), have allowed us to ask more precise questions to identify which ROS are elevated by ABA and where these ROS increases are found within guard cells. In this study, we use both ROS-responsive fluorescent dyes and genetically encoded biosensors combined with spectral unmixing and 3D rendering of Airy scans to demonstrate that ABA increases H_2O_2 within specific subcellular compartments in Arabidopsis guard cells and to understand the signaling and enzymatic machinery that drives synthesis of these ROS.

We examined the dependence of the ABA-induced ROS synthesis on the canonical ABA signaling pathway using the generic ROS dye, CM H_2DCF-DA. We detected significant increases in DCF fluorescence that are temporally coincident with stomatal closure in Col-0 leaves. We examined the response in the quintuple ABA receptor mutant *pyl-11458*. In this mutant ABA-induced guard cell closure and DCF fluorescence increases are reduced relative to Col-0. In contrast in the *abo6* mutant, which was isolated for elevated ABA signaling in roots, both ABA-induced DCF fluorescence and stomatal closure are enhanced. These findings tightly link ABA-elevated ROS in guard cells to stomatal closure.

ABA treatment increased ROS in localized regions in addition to the cytosol, which could be detected by chemical and biosensors. We identified these organelles using DAPI (for the nucleus), chlorophyll autofluorescence (for the chloroplast) and Mitotracker (for the mitochondria). ABA increased the fluorescence intensity of the general ROS probe, DCF, in the

cytoplasm, mitochondria, nuclei, and chloroplasts. The most striking increases observed in the chloroplast and mitochondria.

We asked whether these ABA-dependent increases in DCF fluorescence in these four locations were tied to the previously reported role of RBOH enzymes in ROS signaling in when whole guard cell DCF fluorescence was quantified (Kwak et al., 2003; Drerup et al., 2013; Hsu et al., 2018; Postiglione and Muday, 2020). In Arabidopsis, this ROS increase has been linked to RBOH enzymes using mutants in genes encoding RBOHD and RBOHF (Kwak et al., 2003) and in several species using a relatively nonspecific RBOH inhibitor, Diphenyleneiodonium (DPI) (Watkins et al., 2017). RBOH enzymes have well established roles in hormone induced ROS synthesis in mammals (Vermot et al., 2021) and plants (Chapman et al., 2019). These enzymes produce superoxide in the apoplast, which can be rapidly dismutated into H_2O_2 via superoxide dismutase. The influx of H_2O_2 into the cytoplasm is facilitated by aquaporins, making it available to reversibly oxidize cytoplasmic protein targets to change their conformation, activity and/or regulatory properties (Tian et al., 2016; Rodrigues et al., 2017). Yet, whether RBOH enzymes drive ROS accumulation in guard cells in regions beyond the cytoplasm has not been examined.

To better understand the mechanism behind ROS increases during ABA response, we evaluated spatial localization of DCF in the *rbohd/f* double mutant and after treatment with a RBOH inhibitor. We quantified the levels of ROS in the cytoplasm of this *rbohd/f* double mutant and find that there is a significant decrease in ABA-induced DCF fluorescence relative to Col-0 consistent with the established role of this enzyme in elevated cytosolic ROS. Similarly, treatment with the RBOH specific inhibitor, VAS2870 (Reis et al., 2020), reduces ABA-induced cytosolic ROS and ABA-dependent guard cell closure. We also examined the accumulation of DCF signal in chloroplasts, nucleus, and mitochondria. Intriguingly, in the *rbohd/f* double mutant and after treatment with the highly specific VAS2870 inhibitor (Reis et al., 2020), the ABA-induced signal is no longer significantly different from controls in all three of these locations. This finding both emphasizes the role of RBOH in ABA-induced ROS, but also suggests that RBOH either directly or indirectly increases ROS in cellular locations beyond the cytosol, which is an important insight into the function of this class of signaling driven, ROS synthesizing enzymes. As RBOH activity can ultimately result in elevated levels of H_2O_2 within target cells,

we used additional experimental approaches to verify that the ROS changes detected with DCF included increased H_2O_2.

We used two approaches to quantify H_2O_2 changes, examining both the H_2O_2 responsive cytoplasmic targeted genetically-encoded sensor roGFP2-Orp1 and the H_2O_2-selective chemical probe, PO1. This highly reactive biosensor contains a ratiometric readout which provides advantages over chemical dyes, which can be influenced by differences in dye uptake. Although, this reporter is limited in its ability to detect ROS changes in all cellular locations as its synthesis is targeted to specific compartments. PO1 revealed interesting subcellular ROS accumulation patterns with significantly increased signal in chloroplasts and mitochondria in response to ABA. The chloroplast localization pattern of PO1 is not uniform, so we evaluated its distribution using three-dimensional rendering of these PO1 images showing that signal is internal to this organelle with uneven distribution consistent with localized accumulation within regions of the chloroplast. In contrast, mitochondria show uniform signal. Yet, we were unable to detect significant changes in PO1 in the cytosol even at higher doses of ABA. We therefore examined the highly sensitive genetically encoded roGFP2-Orp1 sensor.

The roGFP2-Orp1 genetically encoded ROS biosensor is a powerful new tool to record H_2O_2 changes in tissues to which it is targeted (Gutscher et al., 2009; Nietzel et al., 2019; Ugalde et al., 2021b) and we were able to detect changes in ABA-induced H_2O_2 with this sensor. This sensor has a cysteine residue that is oxidized by H_2O_2 leading to a conformational change that alters its optical properties. When reduced, the sensor has elevated signal intensity following excitation with the 488 nm laser line, while oxidation leads to elevated signal following 405 nm excitation. The dynamic range of this sensor can be defined by treating with DTT to fully reduce the sensor and H_2O_2 to fully oxidize it. Using this sensor, we reveal that ABA treatment leads to a significant increase in H_2O_2 when fluorescence in the whole guard cell is quantified and when the signal in the cytosol is quantified. Although this biosensor revealed ROS increases in individual cells over time after ABA treatment, the potential for photo-oxidation of guard cell chloroplasts eventually leading to oxidation of the sensor limits its application in real time (Ugalde et al., 2021b). To prevent that effect, we quantified the oxidation using multiple samples each imaged at different times after ABA treatment. This reporter has also been previously shown to accumulate in the nucleus in guard cells (Babbar et al., 2021) and we also detected

ABA-increased ROS accumulation in the guard cell nucleus with this biosensor. Our application of this biosensor reveals that ABA drives H_2O_2 increases in the cytosol and nucleus of guard cells. However, a differently targeted sensor is needed to examine mitochondrial ROS.

The mitochondrial targeted mt-roGFP2-Orp1 (Nietzel et al., 2019) was examined to validate the unexpected ROS increases in this organelle. We then quantified the oxidation state of whole guard cells expressing this reporter in response to ABA treatment, revealing a statistically significant increase in reporter oxidation in guard cells treated with 100 µM ABA. We also stained leaves containing this sensor with PO1 and found that the mitochondria labeled with PO1 displayed strong colocalization with mt-roGFP2-Orp1. This is an exciting new finding linking ABA signaling to the mitochondria in guard cells.

The linkage between ABA and mitochondria has been suggested in roots, when the ability of ABA to inhibit primary root growth was used as the basis of a genetic screen (He et al., 2012; Yang et al., 2014). This approach identified the *abo6* mutant, which has enhanced ABA response and elevated ROS within mitochondria in root cells (He et al., 2012). We examined this mutant and found that it is hypersensitive to ABA with enhanced stomatal closure and increased ROS accumulation relative to Col-0. We find increased ABA-induced stomatal closure, the amount of total ROS accumulation within guard cells, as well as ROS accumulation in guard cell mitochondria of this mutant. The *abo6* mutation maps to a gene encoding a mitochondrial DEXH box RNA helicase that functions in the splicing of several transcripts that are required for proper function of complex I in the mitochondrial electron transport chain. Because complex I is a major source of ROS production, impairment at this site can result in increased electron leakage and thus elevated mitochondrial ROS, though how ABA drives H_2O_2 increases here is not well understood. We also found that the mitochondrial ROS increase following ABA treatment was lost in the *rbohd/f* double mutant, suggesting a link between RBOH-dependent ROS production and ROS accumulation in mitochondria. This finding is consistent with a previous report which found that introduction of the *rbohf* mutation into *abo6* relieved ABA hypersensitivity in *abo6* roots (He et al., 2012). With ROS synthesis in both chloroplasts and mitochondria being tied to metabolic function, a future line of experimentation will be to determine whether ABA signaling interacts with these organelles to specifically upregulate ROS used downstream for signaling, or if ABA is driving altered metabolic rate in these organelles, or both of these responses.

Treatment with ABA led to significant increases in both DCF and PO1 within a second site of metabolic ROS synthesis: chloroplasts. Since chloroplasts generate a substantial amount of ROS during photosynthesis (Foyer and Noctor, 2003; Asada, 2006) it is not surprising that significant increases in signal intensity of both chemical probes were detected in this organelle. ABA-dependent ROS increases in chloroplasts are consistent with previous reports observing ABA-induced increases in DCF in mesophyll and guard cell chloroplasts (Wang et al., 2016), with our study being the first to display increases of H_2O_2 specifically. However, the function of chloroplast ROS increases within the context of ABA-dependent stomatal closure has become an evolving area of interest in recent years. Previous reports have shown mixed responses to chemical inhibition of photosynthetic electron transport, with one report revealing a continued effect of ABA (Wang et al., 2016) and other finding that these inhibitors impair ABA responses (Iwai et al., 2019). Another study showed that a mutant which that lacked chlorophyll in guard cells was still able to close stomata following ABA treatment (Azoulay-Shemer et al., 2015). Therefore, the consequences of ABA-triggered ROS production in guard cell chloroplasts needs further evaluation to reach a clear understanding of its function during stomatal closure.

The nuclei of guard cells showed ABA-dependent increases of DCF fluorescence and roGFP2-Orp1 oxidation, a surprising finding due to limited information on nuclear localized ROS production. This ABA response was reduced in the *rbohd/f* double mutant, suggesting that an RBOH dependent signaling pathway affected accumulation of nuclear ROS. In mammalian systems, NOX1 and NOX4 have been shown to localize within the nucleus to directly affect redox state within this organelle (Chamulitrat et al., 2003; Kuroda et al., 2005; Saez et al., 2016), suggesting that plant RBOHs may function in a similar way. Consistent with ROS synthesizing machinery being localized to the nucleus, previous work utilizing tobacco Bright Yellow-2 suspension cells demonstrated that calcium application was able to trigger ROS production in isolated nuclei (Ashtamker et al., 2007). ROS has also been shown to accumulate in plant nuclei in response to environmental signals via diffusion from the cytosol or as a result of retrograde signaling from other sites of ROS production (Caplan et al., 2015; Exposito-Rodriguez et al., 2017). Increases in ROS within the nucleus may function to regulate the activity of redox-regulated transcription factors with redox regulation identified for members of the WRKY, MYB, NAC, heat shock factors (HSF) families, and ZAT (He et al., 2018). The canonical machinery within the ABA-signaling pathway has previously been shown to regulate

transcriptional cascades in guard cells (Fujita et al., 2011). ABA-dependent upregulation of nuclear ROS may provide an additional level of control over gene expression through changes in oxidation state of specific transcription factors.

The regulation of stomatal aperture in response to environmental stimuli, such as drought, is a crucial process in plant adaptation to stress. This study built on prior evidence that ABA drives ROS increases, identified H_2O_2 as central to this response, as well as revealing the spatial regulation of these ROS. The addition of genetically encoded biosensors to our older toolkit of ROS responsive chemical probes allowed us to overlay the position of ROS accumulation with organelle specific markers to reveal ABA-elevated ROS in the mitochondria. We demonstrated that RBOH enzymes are required for ABA-increased ROS accumulation in the cytoplasm and mitochondria, and that H_2O_2 is sufficient to induce stomatal closure. In support of a function of this mitochondrially derived ROS, a mutant with increased mitochondrial ROS production displayed an increased rate of ABA-induced stomatal closure, suggesting ROS production in this organelle functions in ABA signaling. Together these results indicate that ABA-induced H_2O_2 accumulation exhibits tight spatial regulation that influences stomatal closure and guard cell physiology.

Methods and Materials

Plant Growth Conditions

Arabidopsis thaliana seeds that were used include Col-0, *rbohd/rbohf* double mutant (Miller et al., 2009), *pyl1-1*; *pyr1-1*; *pyl4-1*; *pyl5*; *pyl8-1* quintuple mutant *(pyl-11458)* (Zhang et al., 2020) (ABRC)*, ABA overly sensitive 6* (*abo6)* (Alonso et al., 2003) (ABRC), GFP-PTS1 reporter (Ramón and Bartel, 2010), roGFP2-Orp1 (Nietzel et al., 2019), and mt-roGFP2-Orp1 (Nietzel et al., 2019). Arabidopsis plants were germinated on 1× Murashige and Skoog medium, pH 5.6, Murashige and Skoog vitamins, and 0.8% (w/v) agar, buffered with 0.05% (w/v) MES and supplemented with 1% (w/v) sucrose. After vernalization at 4°C for 48 h, plates were placed under 24-h 120 μmol m^{-2} s^{-2} cool-white light. Seven days after germination, seedlings were transferred to SunGro Redi-Earth Seed Mix. Plants are then grown under a short-day light cycle (8 h light/ 16 h dark) of 120 μmol m^{-2} s^{-2} cool-white light with relative humidity kept between 60-70%. Experiments were conducted on leaves from plants 3 to 4 weeks after germination, unless noted otherwise.

Stomatal Closure Assay

ABA-induced stomatal closure assays were performed with plants 3 to 4 weeks after germination. Epidermal strips were prepared by evenly spraying a microscope slide with a silicone-based medical adhesive (Hollister stock #7730). After 10 min, the abaxial epidermis of the leaf was pressed into the dried adhesive coat, a drop of water was placed on the leaf surface, and the leaf was gently scraped with a razor blade until only the fixed epidermis remains**.** Fresh epidermal peels were then fully covered in opening solution (50 mM KCl, and 10 mM MES buffer, pH 6.15) and incubated under cool-white light (120 µmol m^{-2} s^{-1}) for 3 hrs. To induce stomatal closure, opening buffer was replaced with equal volume of a similar solution with 20 µM or 100 µM ABA added to induce closure. For quantification of stomatal aperture, leaf peels were imaged on an ECHO Revolve microscope using transmitted light. Images were acquired using an Olympus UPlanSApochromat 40x/0.95NA objective.

DCF Staining, Imaging, and Quantification

CM 2,7-dihydrodichlorofluorescein diacetate (CM-H_2DCF-DA) was dissolved in dimethyl sulfoxide to yield a 50-µM stock. This was diluted in deionized water to yield a final concentration of 4.3 µM with 0.1% (v/v) dimethyl sulfoxide. Epidermal peels were prepared, and guard cells were fully opened as described above, then treated with 20 µM ABA or a control buffer. Pre-treatments were fully removed, and the epidermis was stained for 15 min with 4.3 µM H_2DCF-DA stain and washed with deionized water. Microscopy was performed on the Zeiss LSM880 laser scanning confocal microscope with a 32-detector GaAsP array for spectral unmixing. The Plan Apochromat 63x/1.2NA water objective was used for acquisition. The 488 nm laser line was used to excite the leaf surfaces with 0.4% maximum laser power with a 3.5 digital gain. The gain settings were optimized to produce maximum DCF signal while preventing oversaturation. All micrographs were acquired using identical offset, gain, and pinhole settings using the same detectors for each experiment. Settings were defined to spectrally separate the DCF and chlorophyll signal by capturing the emission spectrum for each compound in regions which there was no overlap. Total emission was collected using lambda scanning with a 1 Airy Unit pinhole aperture yielding a 0.9 µm section, the DCF signal alone would later be unmixed from the image for quantification.

Images used for quantification were taken with averaging of 2 with minimal pixel dwell time making sure to limit excess exposure to the laser that may induce ROS. Maximum intensity projections were produced from Z-stacks. The average intensity values within each ROI were acquired and all values obtained were normalized to the average of each subcellular location under control conditions from three biological replicates with 2-3 technical replicates per experiment. DCF fluorescence intensities were measured in ImageJ by drawing ROIs around the whole stomata, chloroplasts, cytosol, nuclei, and mitochondria of multiple guard cells.

The images shown in the figures were captured at high resolution using separate but identically treated samples to those used in the quantification with increased averaging, digital zoom, and pixel dwell time to increase resolution and were not included in any quantification. Individual images were selected that were representative of the magnitude of responses in the images generated for quantification. To produce heat maps, we converted pixel intensities of DCF fluorescence using the look-up tables (LUT) function in the Zen Blue Software.

PO1 Staining, Imaging, and Quantification

Peroxy Orange 1 (PO1) is an H_2O_2 sensor, which was dissolved in dimethyl sulfoxide to yield a 5 mM stock. This was diluted in deionized water to yield a final concentration of 50 µM. Epidermal peels were prepared, and guard cells were fully opened as described above, then treated with 20 µM or 100 µM ABA or a control buffer. Pre-treatments were fully removed, and the epidermis was stained for 30 min with 50 µM PO1 dye and washed with deionized water. Microscopy was performed as described in the above section.

Three-dimensional images of PO1 were acquired on the Zeiss LSM880 system equipped with 32-detector GaAsP array for Airyscan acquisition. Samples were excited with an argon 488 nm laser line using 6% laser power and a Plan Apochromat 63x/1.2NA water objective was used for image acquisition. Total emission was collected using Airyscan of a z-stack spanning the entire depth of a whole guard cell pair, using the optimal optical slice size calculated by the ZEN Black acquisition software. Images were then rendered in three dimensions using Aivia image analysis software. x,y and z,y projections were then acquired of cropped regions containing chloroplasts or mitochondria.

To produce heat maps displayed in Supplemental Figure 3, we converted pixel intensities of PO1 fluorescence using the look-up tables (LUT) function in the Zen Blue Software. PO1 fluorescence intensities were measured in ImageJ by drawing ROIs around the chloroplasts, cytosol, nuclei, and mitochondria of each guard cell. The average intensity values within each ROI were acquired and all values obtained were normalized to the average of each subcellular location under control conditions from three biological replicates with three technical replicates per experiment.

Imaging and Analysis of ROS-Sensitive Genetically Encoded Biosensors

Fully mature Arabidopsis rosettes containing roGFP2-Orp1 or mt-roGFP2-Orp1 were excised and peeled prior to being submerged in stomatal opening buffer to equilibrate for 4 hrs to establish a baseline. Stomatal opening buffer was then removed following equilibration and replaced with a similar solution containing 100 µM ABA for 0, 15, 30, or 45 min. Microscopy was performed on the Zeiss LSM880 laser scanning confocal microscope with a Plan

Apochromat 63x/1.2NA water objective was used to sequentially excite leaf surfaces at 405 and 488 nm with 1% maximum laser power. Emission was recorded between 505–535 nm with a 2.4 Airy Unit pinhole aperture yielding a 2.0 µm section. Images used for quantification were taken with averaging of 1 with minimal pixel dwell time to limit laser-induced oxidation of the sensor. Dynamic range of each sensor was defined by treating equilibrated samples with 20 mM DTT or 10 mM H_2O_2 to determine the maximum reduction or maximum oxidation, respectively.

Images of roGFP2-Orp1 targeted to the cytosol were captured as described above and maximum intensity projections were analyzed in ImageJ by drawing a region of interest in the nucleus or a cytosolic region of each guard cell. Images of mt-roGFP2-Orp1 were analyzed by drawing a region of interest around the entire stomata and thresholding to exclude pixels of background intensity values from each measurement. Ratios were calculated by dividing fluorescence intensity following excitation at 405 nm by fluorescence intensity collected after 488 nm excitation. All individual values obtained were normalized to the average of buffer control treated stomata or the 0-minute timepoint in the case of time courses. Ratiometric micrographs were generated using the Ratio Redox Analysis MatLab program package (Fricker, 2016).

Colocalization of Mitochondria and ROS Chemical Probes

For evaluation of peroxisomal colocalization, Arabidopsis leaves containing PTS1-GFP were peeled and labeled with 50 µM PO1 as described above. For evaluation of mitochondrial colocalization, Col-0 Arabidopsis leaves were peeled and treated with 8.6 µM CM H_2DCF-DA as described above and then 1 µM Mitotracker Red for 15 min. Leaves were then visualized using the Zeiss 880 LSCM device as described earlier. Each signal was resolved in lambda scanning mode, with emission spectra for each individual spectra being obtained prior to colocalization analysis by imaging single labeled samples. Images were taken at multiple Z-positions, though not combined into maximum intensity projections as to not misrepresent colocalization of signals that might be found in the same vertical plane but at different depths. Emission spectra for each signal were then unmixed from corresponding images to better evaluate how either signal contributed to a particular location. For colocalization analysis, samples were examined using the Zeiss Zen colocalization module. The threshold for PO1, GFP-PTS1, DCF, Mitotracker Red, mt-roGFP2-Orp1 was determined in each image, via regions that

contained only one fluorescent signal. Regions of interest surrounding mitochondria in PO1 or DCF were then selected and evaluated for colocalization with either GFP-PTS1, mt-roGFP2-Orp1, or Mitotracker Red. Colocalization was then calculated using Pearson's coefficients (weighted colocalization coefficients) and respective scatterplots were generated.

Statistical Analysis

The data for the subcellular localization of DCF and whole stomata roGFP2-Orp1 quantifications were analyzed via student t-tests using GraphPad Prism 9 comparing ABA to control in each respective cellular location. DCF fluorescence intensities for ABA signaling mutants, widths of stomatal apertures, subcellular PO1 signal intensity, and roGFP2-Orp1 time course data were analyzed by one-way ANOVA using GraphPad Prism 9. This analysis evaluated differences within genotypes between different treatments and compared between genotypes under similar treatments for ABA signaling mutants, between control and multiple ABA treatments for PO1 fluorescence, and between timepoints for roGFP2-Orp1 and mt-roGFP2-Orp1. Tukey's multiple comparison tests were then utilized to resolve significant differences between treatments, genotypes, or timepoints.

Accession Numbers

Sequence data from this article can be found in the GenBank/EMBL data libraries under the accession numbers: *PYR1* (At4g17870), *PYL1* (At5g46790), *PYL4* (At2g38310), *PYL5* (At5g05440), *PYL8* (At5g53160), *ABO6* (At5g04895), *RBOHD* (At5g47910), *RBOHF* (At1g64060).

Acknowledgments

We would like to acknowledge the assistance of Dr Heather Brown Harding (Microscopy core facility) with imaging. We greatly appreciate the generosity of Dr Andreas Meyer and Dr Jose Ugalde in sharing roGFP2-Orp1 and mt-roGFP2-Orp1 seeds, as well as providing helpful feedback on the manuscript. We also thank Dr Gad Miller for providing us with *rbohd/f* seeds and Dr. Bonnie Bartel for the GFP-PTS1 transgenic line, and the ABRC for distributing *pyl-11458* and *abo6* seeds. Lastly, we would like to thank members of the Muday lab for valuable input on the manuscript. This work was funded by NSF IOS-1558046 to G.K.M and a fellowship from the

Center for Molecular Signaling and an NIH T32 GM127261 fellowship to A.E.P. The content is solely the responsibility of the authors and does not necessarily represent the official view of the National Institutes of Health.

Author Contributions

AEP designed experiments, performed research, analyzed data, and wrote the paper. GKM designed experiments, wrote, and edited the paper.

References

Alonso, J.M., Stepanova, A.N., Leisse, T.J., Kim, C.J., Chen, H., Shinn, P., Stevenson, D.K., Zimmerman, J., Barajas, P., Cheuk, R., Gadrinab, C., Heller, C., Jeske, A., Koesema, E., Meyers, C.C., Parker, H., Prednis, L., Ansari, Y., Choy, N., Deen, H., Geralt, M., Hazari, N., Hom, E., Karnes, M., Mulholland, C., Ndubaku, R., Schmidt, I., Guzman, P., Aguilar-Henonin, L., Schmid, M., Weigel, D., Carter, D.E., Marchand, T., Risseeuw, E., Brogden, D., Zeko, A., Crosby, W.L., Berry, C.C., and Ecker, J.R. (2003). Genome-Wide Insertional Mutagenesis of Arabidopsis thaliana. Science (New York, N.Y.) **301,** 653-657.

An, Y., Liu, L., Chen, L., and Wang, L. (2016). ALA Inhibits ABA-induced Stomatal Closure via Reducing H2O2 and Ca2+ Levels in Guard Cells. Frontiers in plant science **7**.

Asada, K. (2006). Production and Scavenging of Reactive Oxygen Species in Chloroplasts and Their Functions. Plant physiology **141,** 391-396.

Ashtamker, C., Kiss, V., Sagi, M., Davydov, O., and Fluhr, R. (2007). Diverse subcellular locations of cryptogein-induced reactive oxygen species production in tobacco Bright Yellow-2 cells. Plant physiology **143,** 1817-1826.

Azoulay-Shemer, T., Palomares, A., Bagheri, A., Israelsson-Nordstrom, M., Engineer, C.B., Bargmann, B.O., Stephan, A.B., and Schroeder, J.I. (2015). Guard cell photosynthesis is critical for stomatal turgor production, yet does not directly mediate CO2 - and ABA-induced stomatal closing. The Plant journal : for cell and molecular biology **83,** 567-581.

Babbar, R., Karpinska, B., Grover, A., and Foyer, C.H. (2021). Heat-Induced Oxidation of the Nuclei and Cytosol. Frontiers in plant science **11**.

Bienert, G.P., Moller, A.L., Kristiansen, K.A., Schulz, A., Moller, I.M., Schjoerring, J.K., and Jahn, T.P. (2007). Specific aquaporins facilitate the diffusion of hydrogen peroxide across membranes. The Journal of biological chemistry **282,** 1183-1192.

Boominathan, P., Shukla, R., Kumar, A., Manna, D., Negi, D., Verma, P.K., and Chattopadhyay, D. (2004). Long term transcript accumulation during the development of dehydration adaptation in Cicer arietinum. Plant physiology **135,** 1608-1620.

Caplan, J.L., Kumar, A.S., Park, E., Padmanabhan, M.S., Hoban, K., Modla, S., Czymmek, K., and Dinesh-Kumar, S.P. (2015). Chloroplast Stromules Function during Innate Immunity. Developmental cell **34,** 45-57.

Chamulitrat, W., Schmidt, R., Tomakidi, P., Stremmel, W., Chunglok, W., Kawahara, T., and Rokutan, K. (2003). Association of gp91phox homolog Nox1 with anchorage-independent growth and MAP kinase-activation of transformed human keratinocytes. Oncogene **22,** 6045-6053.

Chapman, J.M., Muhlemann, J.K., Gayomba, S.R., and Muday, G.K. (2019). RBOH-Dependent ROS Synthesis and ROS Scavenging by Plant Specialized Metabolites To Modulate Plant Development and Stress Responses. Chemical Research in Toxicology **32,** 370-396.

Demidchik, V. (2018). ROS-Activated Ion Channels in Plants: Biophysical Characteristics, Physiological Functions and Molecular Nature. Int J Mol Sci **19,** 1263.

Dickinson, B.C., Huynh, C., and Chang, C.J. (2010). A Palette of Fluorescent Probes with Varying Emission Colors for Imaging Hydrogen Peroxide Signaling in Living Cells. Journal of the American Chemical Society **132,** 5906-5915.

Drerup, M.M., Schlücking, K., Hashimoto, K., Manishankar, P., Steinhorst, L., Kuchitsu, K., and Kudla, J. (2013). The Calcineurin B-Like Calcium Sensors CBL1 and CBL9 Together with Their Interacting Protein Kinase CIPK26 Regulate the Arabidopsis NADPH Oxidase RBOHF. Molecular plant **6,** 559-569.

Exposito-Rodriguez, M., Laissue, P.P., Yvon-Durocher, G., Smirnoff, N., and Mullineaux, P.M. (2017). Photosynthesis-dependent H2O2 transfer from chloroplasts to nuclei provides a high-light signalling mechanism. Nature Communications **8,** 49.

Fahad, S., Bajwa, A.A., Nazir, U., Anjum, S.A., Farooq, A., Zohaib, A., Sadia, S., Nasim, W., Adkins, S., Saud, S., Ihsan, M.Z., Alharby, H., Wu, C., Wang, D., and Huang, J. (2017). Crop Production under Drought and Heat Stress: Plant Responses and Management Options. Frontiers in plant science **8**.

Foyer, C.H., and Noctor, G. (2003). Redox sensing and signalling associated with reactive oxygen in chloroplasts, peroxisomes and mitochondria. Physiologia Plantarum **119,** 355-364.

Foyer, C.H., and Noctor, G. (2020). Redox Homeostasis and Signaling in a Higher-CO2 World. Annual Review of Plant Biology **71,** 157-182.

Fricker, M.D. (2016). Quantitative Redox Imaging Software. Antioxidants & redox signaling **24,** 752-762.

Fujita, Y., Fujita, M., Shinozaki, K., and Yamaguchi-Shinozaki, K. (2011). ABA-mediated transcriptional regulation in response to osmotic stress in plants. Journal of Plant Research **124,** 509-525.

Fukai, T., and Ushio-Fukai, M. (2011). Superoxide dismutases: role in redox signaling, vascular function, and diseases. Antioxidants & redox signaling **15,** 1583-1606.

Gadjev, I., Vanderauwera, S., Gechev, T.S., Laloi, C., Minkov, I.N., Shulaev, V., Apel, K., Inzé, D., Mittler, R., and Van Breusegem, F. (2006). Transcriptomic footprints disclose specificity of reactive oxygen species signaling in Arabidopsis. Plant physiology **141,** 436-445.

Geiger, D., Scherzer, S., Mumm, P., Stange, A., Marten, I., Bauer, H., Ache, P., Matschi, S., Liese, A., Al-Rasheid, K.A.S., Romeis, T., and Hedrich, R. (2009). Activity of guard cell anion channel SLAC1 is controlled by drought-stress signaling kinase-phosphatase pair. Proc Natl Acad Sci U S A **106,** 21425-21430.

Gutscher, M., Sobotta, M.C., Wabnitz, G.H., Ballikaya, S., Meyer, A.J., Samstag, Y., and Dick, T.P. (2009). Proximity-based protein thiol oxidation by H2O2-scavenging peroxidases. The Journal of biological chemistry **284,** 31532-31540.

Halliwell, B., and Whiteman, M. (2004). Measuring reactive species and oxidative damage in vivo and in cell culture: how should you do it and what do the results mean? British journal of pharmacology **142,** 231-255.

He, H., Van Breusegem, F., and Mhamdi, A. (2018). Redox-dependent control of nuclear transcription in plants. Journal of experimental botany **69,** 3359-3372.

He, J., Duan, Y., Hua, D., Fan, G., Wang, L., Liu, Y., Chen, Z., Han, L., Qu, L.J., and Gong, Z. (2012). DEXH box RNA helicase-mediated mitochondrial reactive oxygen species production in Arabidopsis mediates crosstalk between abscisic acid and auxin signaling. Plant Cell **24,** 1815-1833.

Hsu, P.-K., Dubeaux, G., Takahashi, Y., and Schroeder, J.I. (2021). Signaling mechanisms in abscisic acid-mediated stomatal closure. The Plant journal : for cell and molecular biology **105,** 307-321.

Hsu, P.-K., Takahashi, Y., Munemasa, S., Merilo, E., Laanemets, K., Waadt, R., Pater, D., Kollist, H., and Schroeder, J.I. (2018). Abscisic acid-independent stomatal CO₂ signal transduction pathway and convergence of CO₂ and ABA signaling downstream of OST1 kinase. Proceedings of the National Academy of Sciences **115,** E9971-E9980.

Iwai, S., Ogata, S., Yamada, N., Onjo, M., Sonoike, K., and Shimazaki, K.-I. (2019). Guard cell photosynthesis is crucial in abscisic acid-induced stomatal closure. Plant Direct **3,** e00137-e00137.

Kalyanaraman, B., Darley-Usmar, V., Davies, K.J.A., Dennery, P.A., Forman, H.J., Grisham, M.B., Mann, G.E., Moore, K., Roberts, L.J., and Ischiropoulos, H. (2012). Measuring reactive oxygen and nitrogen species with fluorescent probes: challenges and limitations. Free Radical Biology and Medicine **52,** 1-6.

Kuroda, J., Nakagawa, K., Yamasaki, T., Nakamura, K., Takeya, R., Kuribayashi, F., Imajoh-Ohmi, S., Igarashi, K., Shibata, Y., Sueishi, K., and Sumimoto, H. (2005). The superoxide-producing NAD(P)H oxidase Nox4 in the nucleus of human vascular endothelial cells. Genes to cells : devoted to molecular & cellular mechanisms **10,** 1139-1151.

Kwak, J.M., Mori, I.C., Pei, Z.M., Leonhardt, N., Torres, M.A., Dangl, J.L., Bloom, R.E., Bodde, S., Jones, J.D., and Schroeder, J.I. (2003). NADPH oxidase AtrbohD and AtrbohF genes function in ROS-dependent ABA signaling in Arabidopsis. EMBO J **22,** 2623-2633.

Lamaoui, M., Jemo, M., Datla, R., and Bekkaoui, F. (2018). Heat and Drought Stresses in Crops and Approaches for Their Mitigation. Frontiers in Chemistry **6**.

Leshem, Y., and Levine, A. (2013). Zooming into sub-organellar localization of reactive oxygen species in guard cell chloroplasts during abscisic acid and methyl jasmonate treatments. Plant Signal Behav **8,** doi: 10.4161/psb.25689.

Li, Q., Wang, Y.-J., Liu, C.-K., Pei, Z.-M., and Shi, W.-L. (2017). The crosstalk between ABA, nitric oxide, hydrogen peroxide, and calcium in stomatal closing of Arabidopsis thaliana **72,** 1140.

Ma, Y., Szostkiewicz, I., Korte, A., Moes, D., Yang, Y., Christmann, A., and Grill, E. (2009). Regulators of PP2C phosphatase activity function as abscisic acid sensors. Science (New York, N.Y.) **324,** 1064-1068.

Miller, G., Schlauch, K., Tam, R., Cortes, D., Torres, M.A., Shulaev, V., Dangl, J.L., and Mittler, R. (2009). The plant NADPH oxidase RBOHD mediates rapid systemic signaling in response to diverse stimuli. Sci Signal **2,** ra45.

Nietzel, T., Elsässer, M., Ruberti, C., Steinbeck, J., Ugalde, J.M., Fuchs, P., Wagner, S., Ostermann, L., Moseler, A., Lemke, P., Fricker, M.D., Müller-Schüssele, S.J., Moerschbacher, B.M., Costa, A., Meyer, A.J., and Schwarzländer, M. (2019). The fluorescent protein sensor roGFP2-Orp1 monitors in vivo H2O2 and thiol redox integration and elucidates intracellular H2O2 dynamics during elicitor-induced oxidative burst in Arabidopsis. New Phytologist **221,** 1649-1664.

Nilson, S.E., and Assmann, S.M. (2007). The control of transpiration. Insights from Arabidopsis. Plant physiology **143,** 19-27.

Nishimura, N., Sarkeshik, A., Nito, K., Park, S.-Y., Wang, A., Carvalho, P.C., Lee, S., Caddell, D.F., Cutler, S.R., Chory, J., Yates, J.R., and Schroeder, J.I. (2010). PYR/PYL/RCAR family members are major in-vivo ABI1 protein phosphatase 2C-

interacting proteins in Arabidopsis. The Plant journal : for cell and molecular biology **61,** 290-299.

Noctor, G., and Foyer, C.H. (2016). Intracellular Redox Compartmentation and ROS-Related Communication in Regulation and Signaling Plant physiology **171,** 1581-1592.

Park, S.Y., Fung, P., Nishimura, N., Jensen, D.R., Fujii, H., Zhao, Y., Lumba, S., Santiago, J., Rodrigues, A., Chow, T.F., Alfred, S.E., Bonetta, D., Finkelstein, R., Provart, N.J., Desveaux, D., Rodriguez, P.L., McCourt, P., Zhu, J.K., Schroeder, J.I., Volkman, B.F., and Cutler, S.R. (2009). Abscisic acid inhibits type 2C protein phosphatases via the PYR/PYL family of START proteins. Science (New York, N.Y.) **324,** 1068-1071.

Pei, Z.M., Murata, Y., Benning, G., Thomine, S., Klusener, B., Allen, G.J., Grill, E., and Schroeder, J.I. (2000). Calcium channels activated by hydrogen peroxide mediate abscisic acid signalling in guard cells. Nature **406,** 731-734.

Postiglione, A.E., and Muday, G.K. (2020). The Role of ROS Homeostasis in ABA-Induced Guard Cell Signaling. Frontiers in plant science **11**.

Qi, J., Song, C.-P., Wang, B., Zhou, J., Kangasjärvi, J., Zhu, J.-K., and Gong, Z. (2018). Reactive oxygen species signaling and stomatal movement in plant responses to drought stress and pathogen attack. Journal of Integrative Plant Biology **60,** 805-826.

Qu, Y., Song, P., Hu, Y., Jin, X., Jia, Q., Zhang, X., Chen, L., and Zhang, Q. (2018). Regulation of stomatal movement by cortical microtubule organization in response to darkness and ABA signaling in Arabidopsis. Plant Growth Regulation **84,** 467-479.

Ramón, N.M., and Bartel, B. (2010). Interdependence of the peroxisome-targeting receptors in Arabidopsis thaliana: PEX7 facilitates PEX5 accumulation and import of PTS1 cargo into peroxisomes. Mol Biol Cell **21,** 1263-1271.

Reis, J., Massari, M., Marchese, S., Ceccon, M., Aalbers, F.S., Corana, F., Valente, S., Mai, A., Magnani, F., and Mattevi, A. (2020). A closer look into NADPH oxidase inhibitors: Validation and insight into their mechanism of action. Redox Biol **32,** 101466.

Rodrigues, O., Reshetnyak, G., Grondin, A., Saijo, Y., Leonhardt, N., Maurel, C., and Verdoucq, L. (2017). Aquaporins facilitate hydrogen peroxide entry into guard cells to mediate ABA- and pathogen-triggered stomatal closure. Proceedings of the National Academy of Sciences **114,** 9200-9205.

Saez, F., Hong, N.J., and Garvin, J.L. (2016). Luminal flow induces NADPH oxidase 4 translocation to the nuclei of thick ascending limbs. Physiol Rep **4,** e12724.

Scuffi, D., Nietzel, T., Di Fino, L.M., Meyer, A.J., Lamattina, L., Schwarzländer, M., Laxalt, A.M., and García-Mata, C. (2018). Hydrogen Sulfide Increases Production of NADPH Oxidase-Dependent Hydrogen Peroxide and Phospholipase D-Derived Phosphatidic Acid in Guard Cell Signaling. Plant physiology **176,** 2532-2542.

Sirichandra, C., Gu, D., Hu, H.C., Davanture, M., Lee, S., Djaoui, M., Valot, B., Zivy, M., Leung, J., Merlot, S., and Kwak, J.M. (2009). Phosphorylation of the Arabidopsis AtrbohF NADPH oxidase by OST1 protein kinase. FEBS letters **583,** 2982-2986.

Suzuki, N., Miller, G., Morales, J., Shulaev, V., Torres, M.A., and Mittler, R. (2011). Respiratory burst oxidases: the engines of ROS signaling. Current Opinion in Plant Biology **14,** 691-699.

Swanson, S.J., Choi, W.G., Chanoca, A., and Gilroy, S. (2011). In vivo imaging of Ca2+, pH, and reactive oxygen species using fluorescent probes in plants. Annu Rev Plant Biol **62,** 273-297.

Takahashi, Y., Zhang, J., Hsu, P.-K., Ceciliato, P.H.O., Zhang, L., Dubeaux, G., Munemasa, S., Ge, C., Zhao, Y., Hauser, F., and Schroeder, J.I. (2020). MAP3Kinase-dependent SnRK2-kinase activation is required for abscisic acid signal transduction and rapid osmotic stress response. Nature Communications **11,** 12.

Tian, S., Wang, X., Li, P., Wang, H., Ji, H., Xie, J., Qiu, Q., Shen, D., and Dong, H. (2016). Plant Aquaporin AtPIP1;4 Links Apoplastic H2O2 Induction to Disease Immunity Pathways. Plant physiology **171,** 1635-1650.

Tõldsepp, K., Zhang, J., Takahashi, Y., Sindarovska, Y., Hõrak, H., Ceciliato, P.H.O., Koolmeister, K., Wang, Y.-S., Vaahtera, L., Jakobson, L., Yeh, C.-Y., Park, J., Brosche, M., Kollist, H., and Schroeder, J.I. (2018). Mitogen-activated protein kinases MPK4 and MPK12 are key components mediating CO2-induced stomatal movements. The Plant Journal **96,** 1018-1035.

Ugalde, J.M., Schlößer, M., Dongois, A., Martinière, A., and Meyer, A.J. (2021a). The latest HyPe(r) in plant H2O2 biosensing. Plant Physiology **187,** 480-484.

Ugalde, J.M., Fuchs, P., Nietzel, T., Cutolo, E.A., Homagk, M., Vothknecht, U.C., Holuigue, L., Schwarzländer, M., Müller-Schüssele, S.J., and Meyer, A.J. (2021b). Chloroplast-derived photo-oxidative stress causes changes in H2O2 and EGSH in other subcellular compartments. Plant Physiology **186,** 125-141.

Vermot, A., Petit-Härtlein, I., Smith, S.M.E., and Fieschi, F. (2021). NADPH Oxidases (NOX): An Overview from Discovery, Molecular Mechanisms to Physiology and Pathology. Antioxidants (Basel) **10,** 890.

Vishwakarma, K., Upadhyay, N., Kumar, N., Yadav, G., Singh, J., Mishra, R.K., Kumar, V., Verma, R., Upadhyay, R.G., Pandey, M., and Sharma, S. (2017). Abscisic Acid Signaling and Abiotic Stress Tolerance in Plants: A Review on Current Knowledge and Future Prospects. Frontiers in plant science **8**.

Wang, W.H., He, E.M., Chen, J., Guo, Y., Chen, J., Liu, X., and Zheng, H.L. (2016). The reduced state of the plastoquinone pool is required for chloroplast-mediated stomatal closure in response to calcium stimulation. The Plant journal : for cell and molecular biology **86,** 132-144.

Watkins, J.M., Hechler, P.J., and Muday, G.K. (2014). Ethylene-Induced Flavonol Accumulation in Guard Cells Suppresses Reactive Oxygen Species and Moderates Stomatal Aperture. Plant physiology **164,** 1707-1717.

Watkins, J.M., Chapman, J.M., and Muday, G.K. (2017). Abscisic Acid-Induced Reactive Oxygen Species Are Modulated by Flavonols to Control Stomata Aperture. Plant physiology **175,** 1807-1825.

Winterbourn, C.C. (2014). The challenges of using fluorescent probes to detect and quantify specific reactive oxygen species in living cells. Biochimica et biophysica acta **1840,** 730-738.

Wu, X., Qiao, Z., Liu, H., Acharya, B.R., Li, C., and Zhang, W. (2017). CML20, an Arabidopsis Calmodulin-like Protein, Negatively Regulates Guard Cell ABA Signaling and Drought Stress Tolerance. Frontiers in plant science **8,** 824-824.

Xu, Z., Jiang, Y., Jia, B., and Zhou, G. (2016). Elevated-CO2 Response of Stomata and Its Dependence on Environmental Factors. Frontiers in plant science **7**.

Yang, L., Zhang, J., He, J., Qin, Y., Hua, D., Duan, Y., Chen, Z., and Gong, Z. (2014). ABA-mediated ROS in mitochondria regulate root meristem activity by controlling PLETHORA expression in Arabidopsis. PLoS genetics **10,** e1004791-e1004791.

Yun, B.-W., Feechan, A., Yin, M., Saidi, N.B.B., Le Bihan, T., Yu, M., Moore, J.W., Kang, J.-G., Kwon, E., Spoel, S.H., Pallas, J.A., and Loake, G.J. (2011). S-nitrosylation of NADPH oxidase regulates cell death in plant immunity. Nature **478,** 264-268.

Zhang, L., Takahashi, Y., Hsu, P.-K., Kollist, H., Merilo, E., Krysan, P.J., and Schroeder, J.I. (2020). FRET kinase sensor development reveals SnRK2/OST1 activation by ABA but not by MeJA and high CO(2) during stomatal closure. eLife **9,** e56351.

Zhang, X., Zhang, L., Dong, F., Gao, J., Galbraith, D.W., and Song, C.P. (2001). Hydrogen peroxide is involved in abscisic acid-induced stomatal closure in Vicia faba. Plant physiology **126,** 1438-1448.